Science Translational Medicine
AAAS

www.sciencetranslationalmedicine.org/cgi/content/full/9/391/eaal4682/DC1

Supplementary Materials for

The brain microenvironment mediates resistance in luminal breast cancer to PI3K inhibition through HER3 activation

David P. Kodack, Vasileios Askoxylakis, Gino B. Ferraro, Qing Sheng, Mark Badeaux, Shom Goel, Xiaolong Qi, Ram Shankaraiah, Z. Alexander Cao, Rakesh R. Ramjiawan, Divya Bezwada, Bhushankumar Patel, Yongchul Song, Carlotta Costa, Kamila Naxerova, Christina S. F. Wong, Jonas Kloepper, Rita Das, Angela Tam, Jantima Tanboon, Dan G. Duda, C. Ryan Miller, Marni B. Siegel, Carey K. Anders, Melinda Sanders, Monica V. Estrada, Robert Schlegel, Carlos L. Arteaga, Elena Brachtel, Alan Huang, Dai Fukumura, Jeffrey A. Engelman,* Rakesh K. Jain*

*Corresponding author. Email: jain@steele.mgh.harvard.edu (R.K.J.); jeffrey.engelman@novartis.com (J.A.E.)

Published 24 May 2017, *Sci. Transl. Med.* **9**, eaal4682 (2017)
DOI: 10.1126/scitranslmed.aal4682

This PDF file includes:

FIGURE S1

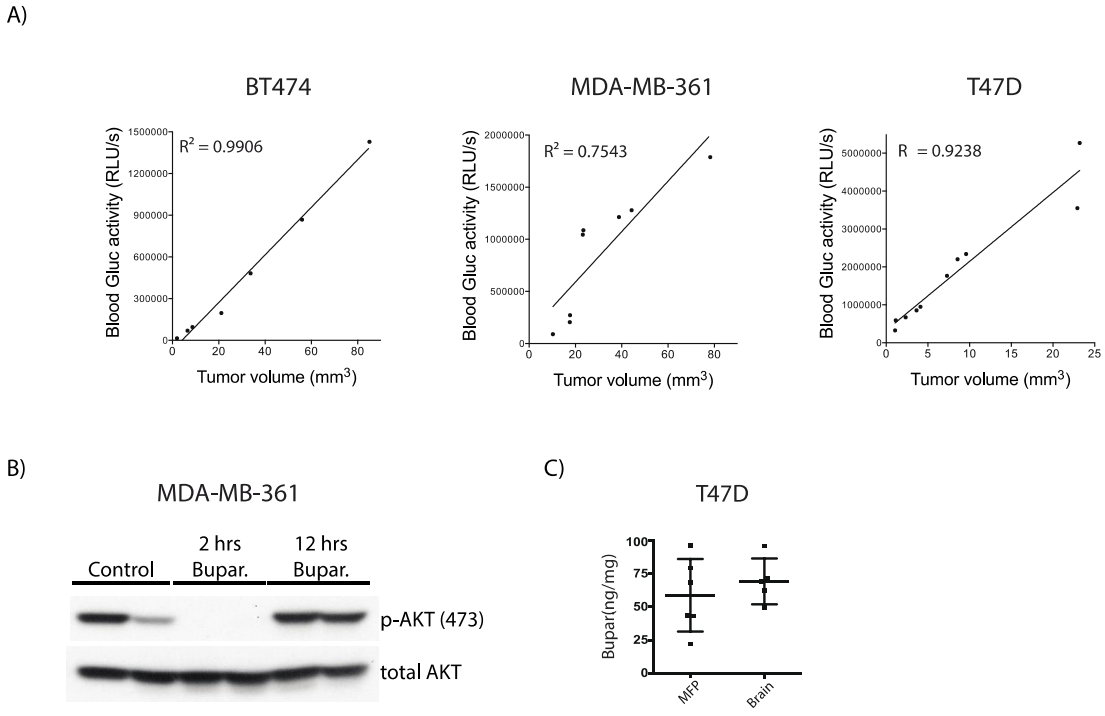

Supplemental Figure 1. **The blood Gluc activity is directly correlated with tumor volume for each tumor model.** (A) Blood Gluc activity is a reliable surrogate for breast cancer brain tumor volume. The correlation of blood Gluc activity and tumor volume, as measured by ultrasound imaging (US), is shown for BT474-Gluc (left) (n=7, Pearson r=0.9953, R^2=0.9906, p<0.0001), MDA-MB-361-Gluc (middle) (n=8, Pearson r=0.8685, R^2=0.7543, 95%-CI=0.42-0.98, p=0.005), and T47D-Gluc (right) (n=10, Pearson r=0.9611, R^2=0.9238, p<0.0001) tumors. (B) MDA-MB-361-Gluc BM tissue, collected at the indicated time points after a single dose of buparlisib, was analyzed for AKT phosphorylation. (C) Concentration of buparlisib in T47D-Gluc tumor tissue collected two hours after treatment.

FIGURE S2

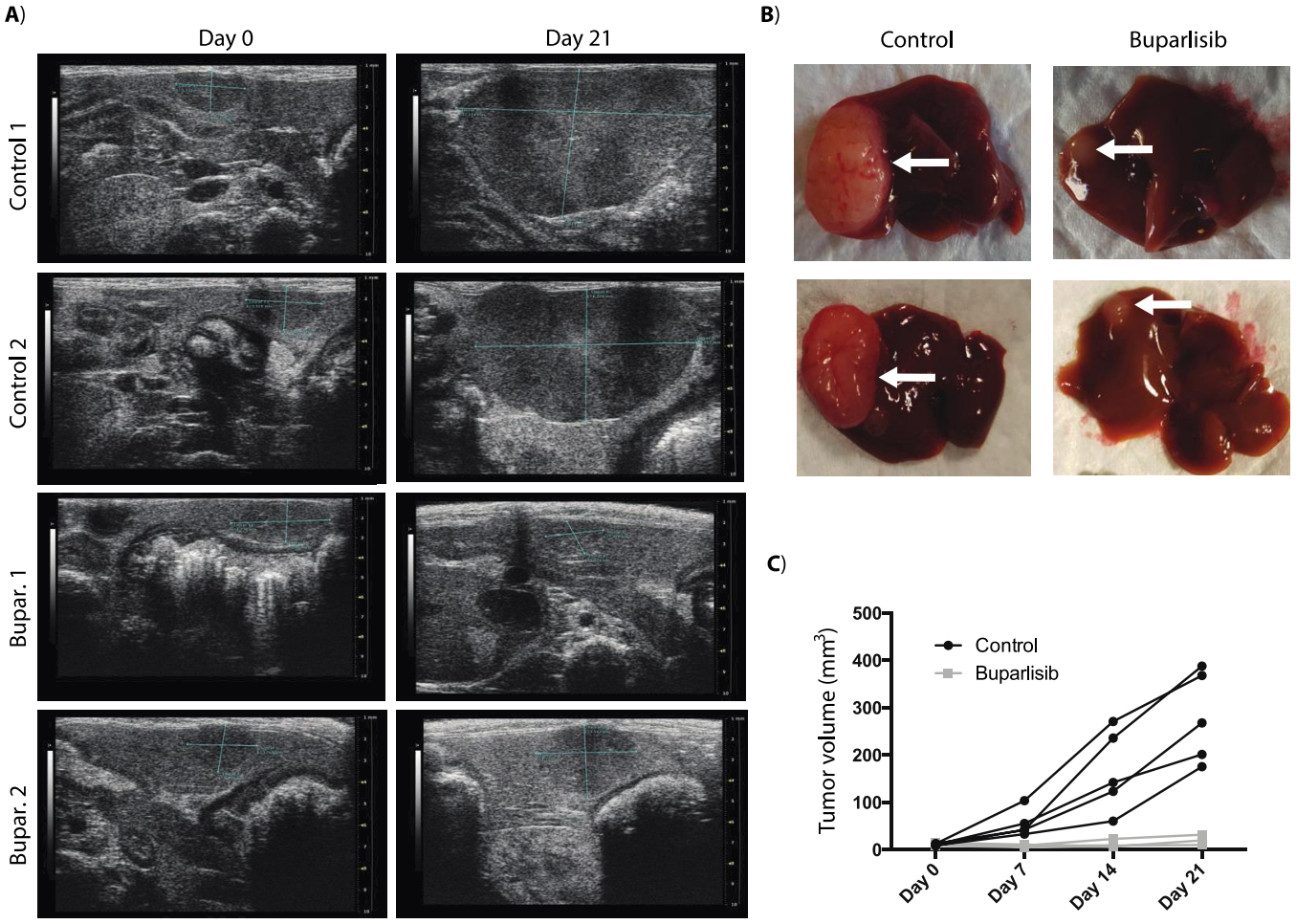

Supplemental Figure 2. Liver BT474 tumors respond to buparlisib. Differential response of established BT474 tumor lesions to buparlisib (BKM120) in the liver of female nude mice. Treatment with buparlisib (50 mg/kg p.o.) was initiated when tumors reached a size of ~10 mm^3, as determined by ultrasound imaging (blue cross). (A) Representative ultrasonography images of size- and time-matched BT474-Gluc tumors treated with vehicle or buparlisib at day 0 and day 21. (B) Representative images of BT474 tumors in resected livers of control or buparlisib-treated mice. Tumor: white arrow. (C) Growth of BT474-Gluc tumors in the liver during treatment with buparlisib (50 mg/kg p.o. daily) or control vehicle (PEG 300) ((n=5).

FIGURE S3

A)

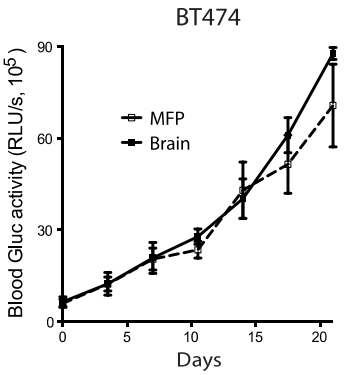

B)

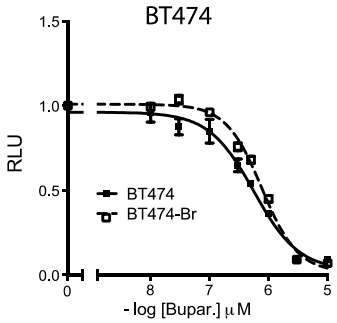

C)

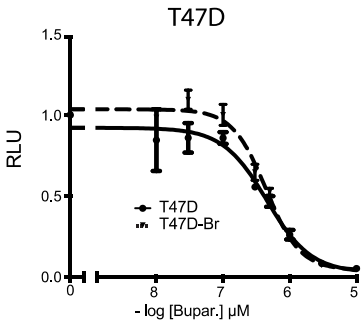

D)

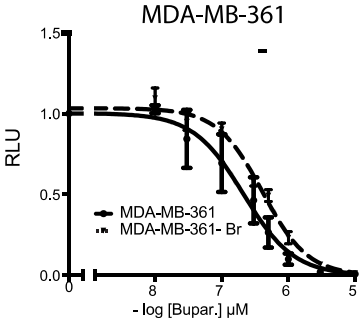

E)

Upregulated in class	Brain
GeneSet	FOXO3_geneset.grp
Enrichment Score (ES)	0.31896326
Normalized Enrichment Score (NES)	1.3047881
Nominal p-value	0.041538462
FDR q-value	0.041538462

F)

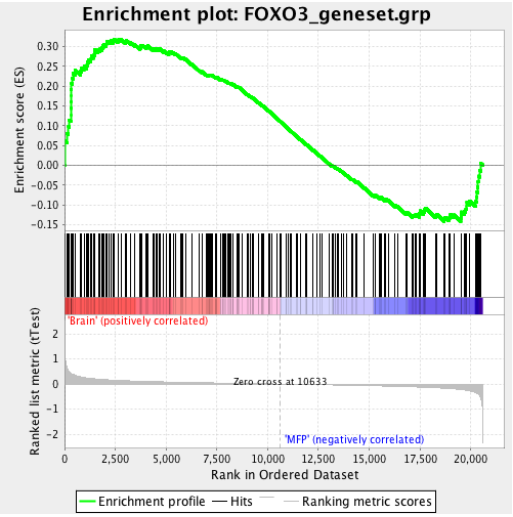

Supplemental Figure 3. Microenvironment-dependent regulation of BC cells alters FOXO3 activity. (A) The growth rate of BT474-Gluc MFP and brain tumors is indistinguishable. (B-D) BT474-Gluc (B), T47D-Gluc (C), and MDA-MB-361-Gluc (D) cells isolated from brain tumors (-Br) are similarly sensitive to PI3K inhibition in vitro as corresponding parental cells (the IC50, unpaired t-test, n=3, ns). (E) Gene set enrichment analysis results for a custom set of genes regulated by FOXO3 TF. (F) Enrichment plot showing that FOXO3a targets are up-regulated when BT474 tumors are grown in the brain vs. the MFP. FDR q-value <0.05.

FIGURE S4

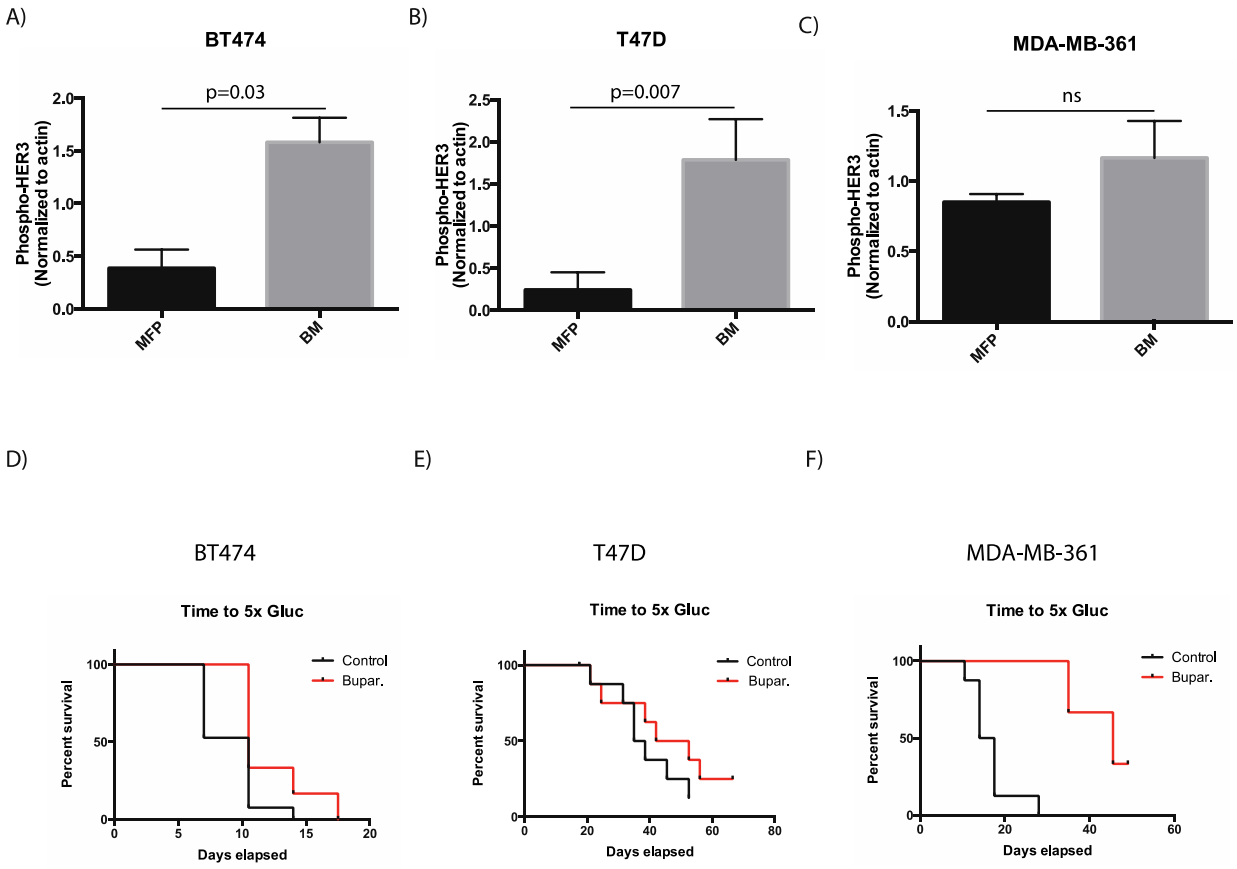

Supplemental Figure 4. MDA-MB-361 brain lesions transiently respond to buparlisib. (A-C) Quantification of phosphorylated HER3 by Western blot (normalized to β-actin) (unpaired t-test, n=3) in BT474 (A), T47D (B), and MDA-MB-361 (C). (D-F) Time to 5x Gluc as surrogate for tumor progression of BT474 (n=19 for control, n=6 for buparlisib), T47D (n=9 per group), and MDA-MD-361-Gluc (n=8 for control, n=6 for buparlisib) BM during treatment with buparlisib or control vehicle (PEG 300). The hazard ratio for MDA-MB-361-Gluc tumors was 0.21 (95%-CI=0.06-0.72), whereas the HRs for BT474-Gluc and T47D-Gluc tumors were 0.53 (95%-CI=0.22-1.24) and 0.59 (95%-CI=0.20-1.79), respectively.

FIGURE S5

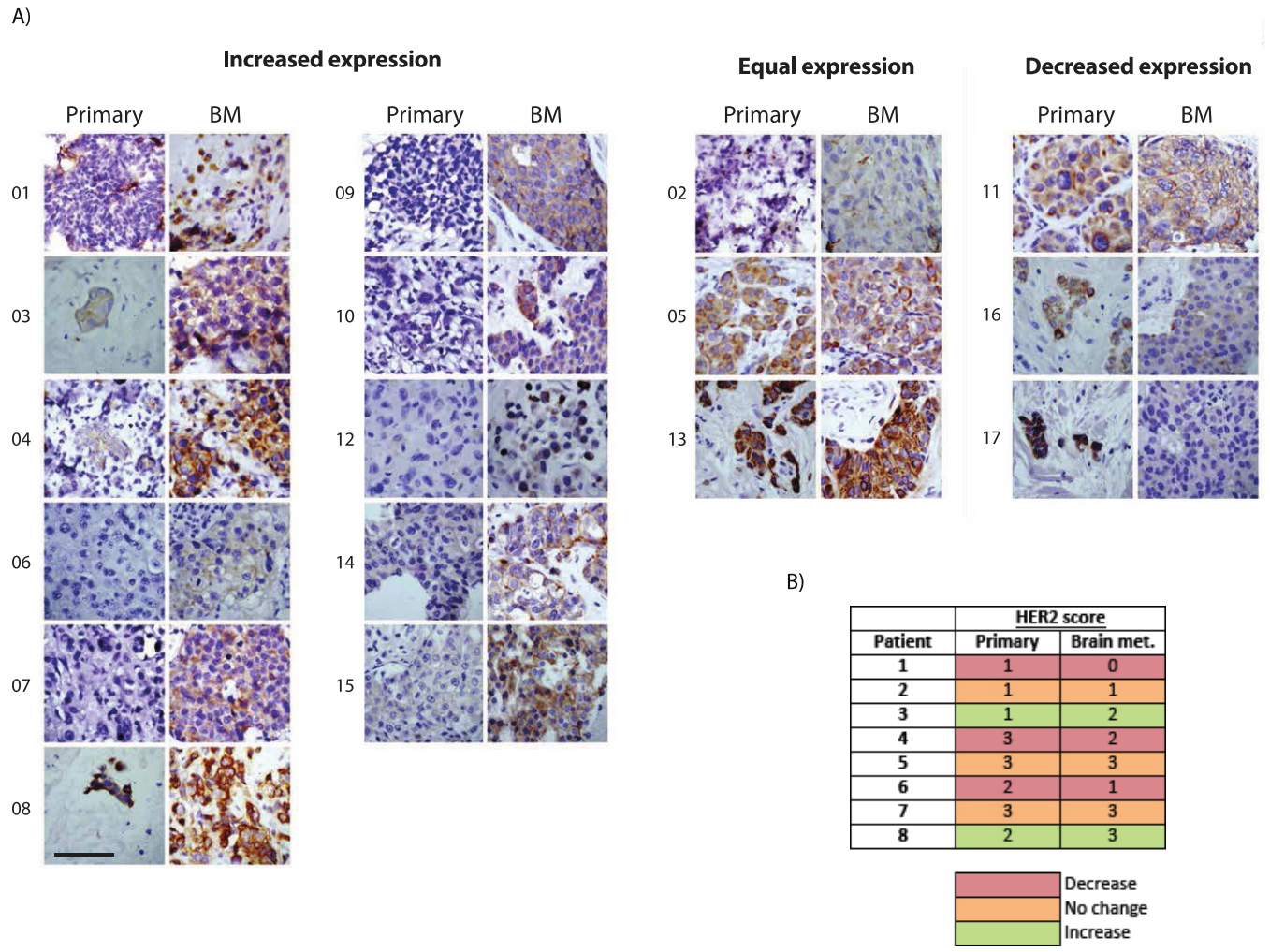

Supplemental Figure 5. HER3 expression is increased in BMs from HER2-positive BC. (A) Representative IHC images for matched human primary and brain metastatic HER2-positive breast tumor tissue stained for HER3 (scale bar = 200 μm). (B) Quantification of whole tissue section IHC analysis of HER2 protein in matched human primary and brain metastatic HER2-positive breast tumor tissue.

FIGURE S6

A)

NRG1 and NRG2 isoforms included in the screen			
GENE_SYMBOL	GENE_DESCRIPTION	NM_FROM_GWC	PROTEIN_REFSEQ_ACC
NRG1	Homo sapiens neuregulin 1 (NRG1), transcript variant SMDF, mRNA	NM_013959.3	NP_039253.1
NRG2	Homo sapiens neuregulin 2 (NRG2), transcript variant 1, mRNA	NM_004883.2	NP_004874.1
NRG2	Homo sapiens neuregulin 2 (NRG2), transcript variant 2, mRNA	NM_013981.3	NP_053584.1
NRG1	Homo sapiens neuregulin 1 (NRG1), transcript variant HRG-beta2, mRNA	NM_013957.3	NP_039251.2
NRG2	Homo sapiens neuregulin 2 (NRG2), transcript variant 3, mRNA	NM_013982.2	NP_053585.1
NRG1	Homo sapiens neuregulin 1 (NRG1), transcript variant SMDF, mRNA	NM_013959.3	NP_039253.1
NRG1	Homo sapiens neuregulin 1 (NRG1), transcript variant HRG-beta1, mRNA	NM_013956.3	NP_039250.2
NRG1	Homo sapiens neuregulin 1 (NRG1), transcript variant HRG-beta3, mRNA	NM_013958.3	NP_039252.2
NRG1	Homo sapiens neuregulin 1 (NRG1), transcript variant HRG-gamma, mRNA	NM_004495.3	NP_004486.2
NRG1	Homo sapiens neuregulin 1 (NRG1), transcript variant ndf43, mRNA	NM_013960.3	NP_039254.1
NRG1	Homo sapiens neuregulin 1 (NRG1), transcript variant HRG-alpha, mRNA	NM_013964.3	NP_039258.1

B)

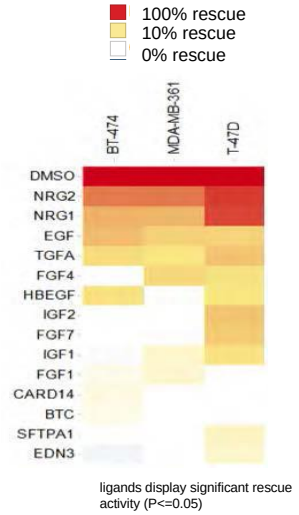

C)

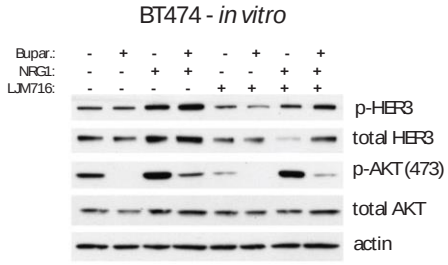

Supplemental Figure 6. Several NRG isoforms induce resistance to buparlisib. NRGs induce resistance to PI3K inhibition in BT474, MDA-MB-361, and T47D breast cancer cells. (A) List of NRG-1 and -2 isoforms used in growth factor screen. (B) List of secreted proteins that display significant in vitro rescue activity of indicated breast cancer cells from buparlisib. The statistical probability score of the rescue % value was also calculated: p-value = Chidist [Z(drug+supe)2, 1]. Secreted proteins that had rescue ≥20% with $P \leq 0.05$ were labeled in each scatter plot (Fig. 3A). (C) Analysis of HER3 and AKT phosphorylation in HER2-amplified BT474-Gluc cells (in vitro) untreated or treated for 2 hours with NRG1, buparlisib, LJM716, or their combination.

FIGURE S7

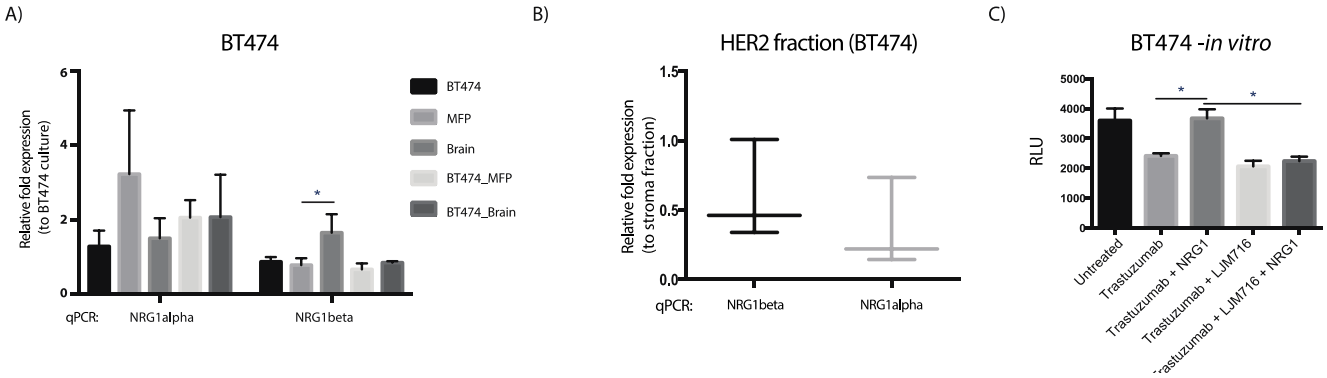

Supplemental Figure 7. NRG-1 is expressed in MFP and brain lesions. (A) Quantification of *NRG1* α and β mRNA in the MFP or brain (normal and BT474 tumor) of athymic nude mice relative to cultured BT474 cells (n = 3 per group, unpaired t-test, *p=0.0123). (B) Quantification of *NRG1* α and β mRNA in HER2-positive BT474 cells from BM enriched by FACS, relative to HER2-negative stromal cells (n = 3 per group). (C) CellTiter-Glo luminescence viability measurements of BT474-Gluc cells exposed to the indicated conditions for 5 days (RLU/s, Relative Light Units per second). (One-way ANOVA, n=3, *p<0.05). Data are displayed as mean ± SD.

TABLE S1

Supplemental Table 1. Differential expression of HER3 in intracranial and extracranial lesions from unmatched patient clinical samples. IHC analysis of HER3 protein in unmatched human primary, extracranial, and brain metastatic HER2-positive breast tumor tissue.

	HER3 score	Primary (N=10)	Extracranial (N=9)	Brain (N=13)
HER3	**0**	5	1	0
	1	2	4	5
	2	2	2	7
	3	1	7	1

TABLE S2

Supplemental Table 2. List of recombinant human growth factors screened for their ability to induce resistance to buparlisib.

A1BG	EGFL6	GPC3	LTA	RNASE1	VCAN
A2M	ELAC1	GPC5	MAPRE1	S100A13	VEGFA
AMH	ELN	GRN	MEPE	SC65	VEGFB
ANGPTL4	EREG	HBEGF	MFAP	SDC1	VEGFC
ANK1	ESM1	HGF	MMP13	SDC2	VGF
AREG	FBLN2	HMSD	MRPL52	SDC4	WISP1
ARTN	FBLN5	HSD17B3	MSTN	SERPINA9	WNT1
BCAN	FGF1	IFNA10	MTRF1L	SERPINB2	WNT10A
BGLAP	FGF10	IFNA13	MUC3A	SERPINH1	WNT10B
BMP1	FGF10	IFNA14	NDP	SFTPA	WNT11
BMP10	FGF12	IFNA16	NODAL	SGCD	WNT2
BMP15	FGF13	IFNA17	NOV	SHH	WNT2B
BMP2	FGF16	IFNA2	NRG1	SNED1	WNT3A
BMP3	FGF17	IFNA21	NRG2	SPOCK1	WNT4
BMP4	FGF19	IFNA5	NRG3	SPOCK2	WNT5A
BMP5	FGF20	IFNA6	NRG4	SPOCK3	WNT5B
BMP6	FGF21	IFNA7	NRP1	SPRY1	WTN6
BMP7	FGF22	IFNA8	NRP2	SPRY2	WNT7A
BTBD17	FGF23	IFNB1	NRTN	SPRY3	WNT7B
BTC	FGF3	IFNW1	OGN	ST3GAL3	WNT8A
C1QTNF4	FGF4	IGF1	OMD	TBC1D28	WNT8B
CARD14	FGF5	IGF2	OPTC	TCN2	WNT9A
CSF1	FGF7	IHH	ORM1	TGFA	WNT9B
CSF2	FGF8	IL10	OSTN	TGFB1	
CTGF	FGF9	IL17RE	PDGFA	TGFB3	
CTSH	FGFBP1	IL1A	PDGFB	THPO	
CYR61	FGG	IL2	PDGFD	TMEFF1	
DEFB1	FGL1	IL21	PDGFRA	TMEFF2	
DEFB136	FIBP	IL26	PDGFRB	TMEM99	
DHH	FLJ37512	IL3	PGF	TNFSF10	
EDN1	FLT3LG	IL34	PIGF	TNFSF11	
EDN2	FRS2	IL4	PILRB	TNFSF12	
EDN3	GDF10	IL6	POFUT1	TNFSF13	
EFNA1	GDF15	ITFG1	POFUT2	TNFSF14	
EFNA2	GDF2	KISS1	PROK1	TNFSF4	
EFNA3	GDF3	KITLG	PSIP1	TNFSF8	
EFNA4	GDF5	LECT1	PTX3	TNFSF9	
EFNA5	GDF6	LECT2	RELT	TPO	
EFNB2	GDF9	LEFTY1	RETN	TSLP	
EFNB3	GDNF	LEFCT2	RHEGF	UBA5	